Similarities in Lithium Growth at Vastly Different Rates

Julian Becherer, Dominik Kramer,* and Reiner Mönig[a]

Lithium electrodeposition is important for lithium metal batteries and is presently a safety and reliability concern for the lithium-ion technology. In the literature, many models for the growth of dendrites can be found and a strong dependence on deposition rate is expected. To elucidate the process of the lithium deposition, *operando* light microscopy at the physical resolution limit of light was performed at rates varying by more than three orders of magnitude. The results show different growth regimes depending on the rate, and where needles, bushes, or accelerated bushes dominate the deposition. All these deposits are based on small crystalline needles and flakes. Little evidence for concentration gradient driven deposition was found. At the highest rate, the electrolyte ionically depletes, but the deposition continues by non-directional bush growth mainly from their insides. An important step at all rates is the insertion into defects in the crystalline lithium.

1. Introduction

The electrodeposition of lithium or other alkaline metals as well as measures of preventing or minimizing their dendritic growth have attracted considerable research efforts. They have been summarized in a relatively large number of highly-cited reviews.[1–8] These include the book of Zhang *et al.*,[1] the reviews of Lin *et al.*[2] and Cheng *et al.*[3] (both cited about 2000 times), and the very recent reviews of Xie *et al.*,[4] Um and Yu,[5] or Zou *et al.*[6]

Although the term dendrite describes a multi-branched structure and lithium deposits usually do not show such a structure, the term dendrite is widely used in literature for different forms of lithium deposits. Therefore, this term is also used here when referred to literature. Many different models for the basic growth mechanisms of dendrites and of lithium deposits were proposed. A selection of these mechanisms/models are briefly summarized in the following.

In 1990 Chazalviel[9] showed that metallic electrodeposition in dilute salt solutions is governed by the space charge created by the depletion of the active species in the vicinity of the electrode on which the metal is deposited. It was shown that the tips of the deposits grow at the velocity of the anions, which is determined by their mobility and the electric field in the neutral region of the electrolyte. The dendritic growth in lithium polymer cells was studied in the framework of Chazalviel's model.[10,11] Brissot *et al.*[10] observed lithium dendrites to grow in the proximity of the velocity predicted by

Chazalviel at high current densities with large inter-electrode distances. In this case, the cell potential exhibited Sand's behavior:[12] after the Sand's time τ, the cationic concentration in the vicinity of the negative electrode drops to zero and the electrolyte becomes ionically depleted. The cationic concentration can only drop to zero if a limiting current density is exceeded. This limiting current density can be calculated with $J_{\mathrm{lim}} = \frac{2z_c c_0 FD}{L(1-t_c)}$[13–15] where z_c is the cationic charge number, c_0 the initial salt concentration in the electrolyte, F the Faraday's constant, D the salt diffusion coefficient, L the inter-electrode distance, and t_c the cationic transference number. If the current density J exceeds the limiting current density J_{lim}, the Sand's time can be calculated with $\tau_{\mathrm{Sand}} = \pi D \left(\frac{z_c c_0 F}{2J(1-t_c)} \right)^2$.[13,14,16] In the experiments of Rosso *et al.*,[11] Sand's behavior was not expected due to their lower current densities, but dendritic growth was still observed at onset times similar to Sand's time. These surprising results were attributed to local inhomogeneities at the surface of the electrode and hence a non-uniform distribution of the concentration. Barton and Bockris[17] studied the growth of silver dendrites and showed that growth is preferred at the tip of protrusions and explained this by the fact that spherical diffusion is faster than linear diffusion. This model was later adapted for lithium polymer cells[15] and lithium deposition in liquid electrolytes.[18] Dendritic growth caused by spherical diffusion can occur at current densities below the limiting current density J_{lim}.

Cohen *et al.*[19] attribute the formation of lithium dendrites to the non-uniformity of the solid-electrolyte interphase (SEI). Due to the lower ionic conductivity of the SEI compared to the liquid electrolyte, the metal will preferably deposit in locations with cracks in the SEI, under thin SEI layers, and in regions in which the non-uniform SEI has the highest ionic conductivity. Wood *et al.*[20] also described fractured and thinned SEI layers as dominant factors for de deposition and dissolution behavior of lithium. Yamaki *et al.*[21] were the first group that reported that lithium deposits grow from the base and not at the tip and compared this growth mechanism to that of tin whiskers. They assumed that the non-uniform deposition of lithium under the SEI induces mechanical stress to the lithium anode that causes

[a] J. Becherer, Dr. D. Kramer, Dr. R. Mönig
    Institute for Applied Materials,
    Karlsruhe Institute of Technology
    Hermann-von-Helmholtz-Platz 1, 76344 Eggenstein-Leopoldshafen, Germany
    E-mail: dominik.kramer@kit.edu

ChemElectroChem

Articles
doi.org/10.1002/celc.202100870

Chemistry Europe
European Chemical
Societies Publishing

the transport of lithium atoms within the electrode. The SEI breaks at a certain point due to surface stress in the electrode and lithium is extruded through these cracks to form whiskers. Also, a more recent work describes the growth of lithium whiskers by a similar mechanism.[22] It was shown by Steiger et al.[23] that the insertion into lithium filaments can occur at the base, at kinks, or in a region close to the tip. A defect-based insertion was suggested as the dominating growth mechanism.

The different theories to describe the growth mechanism of lithium deposits found in literature are often contradictory and not in agreement with experimental results. This is supported by various, partly very recent, reviews, which conclude that there is an insufficient understanding of the plating mechanisms in lithium metal batteries.[2,4,6,24] The models based on ionic concentration gradients and spherical diffusion could only be valid for growth occurring directly at the tip. However, various experimental studies have shown that the growth of deposits did not or not solely occur at the tip.[14,21–23,25–27] Models based only on the non-uniformity of the SEI cannot explain one dimensional growth of needles with constant diameter as observed by Steiger et al.[23] or Kushima et al.[22] As freshly deposited metal necessarily exhibits a thin SEI, deposits would grow three dimensionally when the growth mechanism is solely dominated by the non-uniformity of the SEI. Yamaki's whisker-like growth model was criticized by Monroe and Newman[15] for broad assumptions about the flow behavior of lithium. Defect-based lithium insertion[23] can explain many aspects of the experimentally observed lithium deposition. The electrochemical deposition of lithium was compared with lithium deposition by thermal evaporation in vacuum and showed similar needle-like deposits.[27] This demonstrates that neither an electrolyte nor an SEI are necessary to form lithium needles, which indicates that it is an intrinsic behavior of this metal to form such structures at room temperature.

Numerous recent reviews see a necessity in new *operando* methods for a better understanding of the growth mechanisms of lithium.[2,4–7,24] In this work, very fast *operando* light microscopy is used to observe the deposition of lithium metal. In contrast to other *operando* methods, light microscopy enables experiments in environments very similar to practical applications with a low impact on the electrochemical behavior. Even in cases where x-ray photons and electrons do not cause pronounced beam damage, primary and secondary electrons will locally affect charge and chemistry. Fast microscopic image acquisition allows experiments at very high speed and large observed areas mitigate the risk of misinterpreting the observation of local artifacts. In conventional light microscopy, the depth of field reduces quadratically with an increasing lateral resolution and the value of observations of three-dimensional structures with a low depth of field is limited. Here we use a focus stacking algorithm to acquire images with the highest possible lateral resolution and a large sample volume that is in focus. With this method, it is possible to observe the complete area of the electrode during the *operando* measurements at high resolution.

The growth mechanisms suggested in literature are vastly different. They range from defect-based insertion, taking place at low rates, to ionic depletion in the electrolyte and tip growth at the highest rates possible. Therefore, one mechanism may not be able to explain the electrodeposition of lithium at all rates. Instead, several mechanisms are expected to contribute. Further, it seems highly likely that at different rates or stages of growth, different mechanisms dominate the deposition. So far, only a limited number of publications focus on the selection of different growth modes under different conditions. To the best of the authors knowledge, only Bazant's group[14,22] and Yamaki et al.[21] describe the transition between different basic growth mechanisms in detail. Bai et al.[14] observed a transition from mossy lithium growing from the base to a dendritic tip-growth after Sand's time. Kushima et al.[22] later studied the growth from the base in more detail by *in situ* TEM experiments and differentiated between a dense growth of bud-like protrusions at low overpotentials and a stress driven whisker growth at higher overpotentials. Yamaki et al.[21] described a transition from whisker-like growth to defect-based insertion at the tip and kinks when the electrode is covered with long whiskers, hindering the ion transport to the surface of the electrode. Steiger et al.[25] described a transition from the growth of lithium filaments to lithium moss by the multiplication of insertion defects. Both were attributed to a defect-based insertion and hence cannot be considered as a change of the basic growth mechanism.

We investigate lithium electrodeposition and identify how the deposition process depends on the deposition rate. Our microscopy technique is capable of fast measurement. We can monitor a large volume of the cell at high resolution (~ 500 nm) within a short time. This makes our experimental method ideal for revealing the effect of rate during electrodeposition. In this work, the rate was varied by more than three orders of magnitude, covering all realistic rates used in non-thermal batteries.

2. Results

Here we compare the electrodeposition of lithium on lithium on a copper substrate at different rates. Before the experiments, an electrochemical pretreatment was used to cover the electrode with a dense lithium film. This consisted of a seeding step and a deposition of $0.5\ mAh\ cm^{-2}$ at a rate of $-0.5\ mA\ cm^{-2}$. After the pretreatment, a different deposition rate was applied to each cell and the deposition was imaged *operando*. The deposition rates investigated in this report are $-0.05\ mA\ cm^{-2}$, $-0.5\ mA\ cm^{-2}$, $-2.5\ mA\ cm^{-2}$, $-5\ mA\ cm^{-2}$, and $-10\ mA\ cm^{-2}$. Generally, a total charge per area of $5\ mAh\ cm^{-2}$ (only $4.5\ mAh\ cm^{-2}$ for $-0.5\ mA\ cm^{-2}$) was deposited. Additionally, higher deposition rates of $-50\ mA\ cm^{-2}$ and $-100\ mA\ cm^{-2}$ were applied in a test cell with a larger inter-electrode distance to achieve complete lithium ion depletion at the surface of the working electrode.

Figure 1a shows a light microscopy image of the electrode after the electrochemical pretreatment. The electrode is fully covered by lithium. The deposit that is generated can be seen at higher resolution in Figure 1b. The scanning micro-
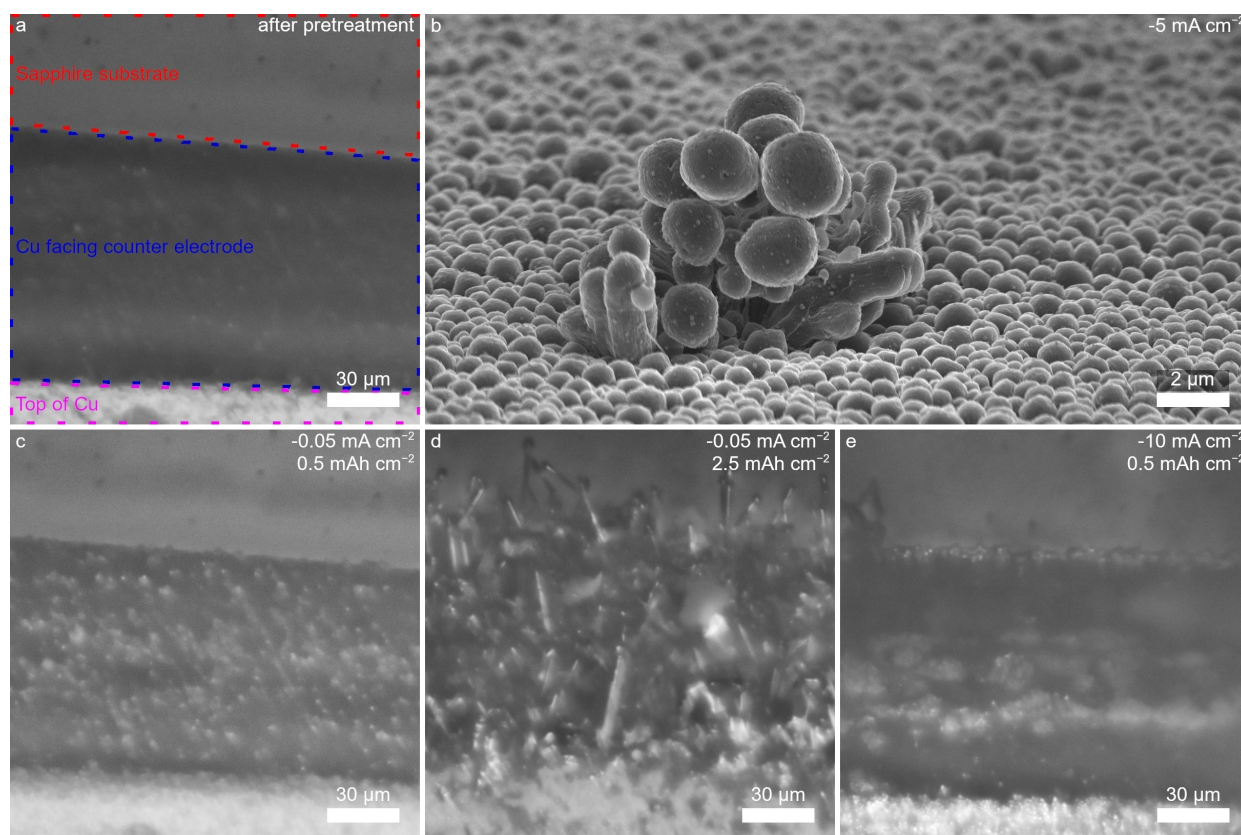
ChemElectroChem

Articles
doi.org/10.1002/celc.202100870

**Chemistry
Europe**
European Chemical
Societies Publishing

Figure 1. (a) Copper electrode after the standard pretreatment (nucleation and the deposition of 0.5 mAh cm^{-2} at -0.5 mA cm^{-2}). (b) SEM image of initial bush growth at -5 mA cm^{-2} on a dense layer of lithium spheres (5 mAh cm^{-2} deposited after pretreatment). The same area of the electrode from a after an additional deposition of 0.5 mAh cm^{-2} (c) and 2.5 mAh cm^{-2} (d) at -0.05 mA cm^{-2}. (e) Copper electrode after pretreatment and the deposition of 0.5 mAh cm^{-2} at -10 mA cm^{-2}.

scopy (SEM) image in Figure 1b shows the early stage of a protrusion but away from this site, the result of the pretreatment can be clearly seen: It consists in a surface fully covered by close packed lithium spheres. The growth of the layer during the pretreatment is shown in the supporting information (section A1). The layer thickness measured with the light microscope is approximately in agreement with a layer of randomly close packed equal spheres. We assume that the result of each pretreatment of the copper electrode leads to this morphology of the lithium electrode which consist of densely packed spheres such as the one shown in Figure 1b.

Figure 1c–e compares the lithium deposits that grew after the pretreatment at two very different rates. The growth at our lowest deposition rate of -0.05 mA cm^{-2} was observed *operando* with the light microscope and is shown in Figure 1c and d and the supporting video SV1. After 10 h at -0.05 mA cm^{-2} the lithium deposit is considerably rougher compared to the pretreated electrode but evenly distributed over the full electrode and no needles are visible (c). After 50 h of deposition, the electrode is fully covered by long lithium needles (d). In contrast to the rather evenly distributed deposits on the electrode surface at the low rate, the deposition is more localized at higher rates (Figure 1e and supporting video SV2). Although the area specific charge in Figure 1c and e are the same, the deposits appear to be very different. At the rate of

-10 mA cm^{-2} bushes start to grow at different locations immediately from the beginning of the deposition. In addition to the bush growth in the middle of the electrode (Figure 1e), a very fast-growing bush that initiates from the edge of the electrode is visible in the video SV2. It quickly dominates the whole deposition process and soon grows out of the large focus range that was used.

The fast growth of a bush that dominates the deposition was also observed at lower current densities but did not initiate directly at the start of the deposition as described before for -10 mA cm^{-2}. The *operando* observation of the deposition at -2.5 mA cm^{-2} is shown in Figure 2 and the supporting video SV3. The images in Figure 2a, b, and c were recorded after a deposition of charges of 0.67 mAh cm^{-2}, 1.33 mAh cm^{-2}, and 2 mAh cm^{-2}, respectively. Figure 2d shows the cell voltage vs. time with marks at the times when the images a-c was taken. An enhanced deposition is apparent at the lower edge of the copper block close to the substrate (Figure 2a) and especially at the upper edge where a long dense bush with a cylindrical shape grows (surrounded by the short-dashed line). To visualize the enhanced deposition, the inset in Figure 2a shows a schematic cross section along the long-dashed line. The small bump in the lower right of the inset depicts the deposits at the lower edge and the round lithium deposits at the top of the inset (highlighted with the dashed line) illustrates the enhanced
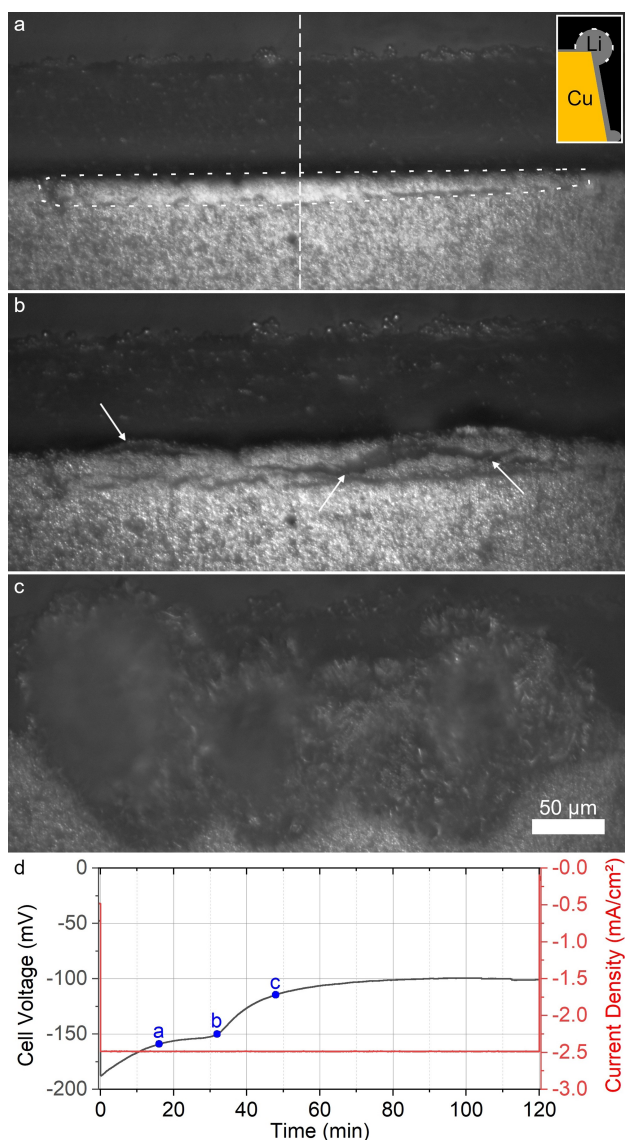
ChemElectroChem

Articles
doi.org/10.1002/celc.202100870

**Chemistry
Europe**

European Chemical
Societies Publishing

Figure 2. *Operando* light microscopy images of the working electrode after 16 min (a), 32 min (b), and 48 min (c) of Li deposition at $-2.5\ \mathrm{mA\,cm^{-2}}$. (d) Galvanostatic voltage vs. time trace with markers that indicate when the images a–c was taken. The short-dashed line (a) highlights the preferred deposition at the upper edge in cylindrical shape and the long-dashed line indicates an exemplary cross section location for the schematic inset. The arrows (b) highlight the occurring parting in the deposit.

deposition along the upper edge of the copper block in cylindrical shape. The deposition on this dense bush appears faster than in other regions of the electrode, but despite the faster growth, the growth of the dense bush itself is very steady for approximately 30 minutes. However, after slightly more than 30 minutes, a parting in the bush opens up (highlighted by arrows in Figure 2b) and the bush starts to grow very fast (Figure 2c). The deposition in all other areas of the electrode almost comes to stop after the dense bush parts open and transitions to a fast-growing bush with a more porous structure. The drop in the overpotential of the galvanostatic voltage trace (Figure 2d) correlates very precisely with the change from a slow and dense to a fast-growing porous bush. This correlation

between cell voltage and deposition morphology was observed in all cells in which a sudden bush growth dominated deposition. In the cell where lithium was deposited at a rate of $-5\ \mathrm{mA\,cm^{-2}}$, the fast bush growth initiated on the top of copper electrode at the edge of the rubber seal (supporting video SV4), which is the location farthest away from the lithium counter electrode. Therefore, it can be excluded that the drop in overpotential is associated with a reduction of the inter-electrode distance. Although the large bushes in the supporting videos SV2, SV3, and SV4 partly grow out of focus, it can be clearly observed that none of them shows a tip-growth behavior but rather a three-dimensional volumetric growth mechanism that was previously reported and compared to the rising dough of a raisin bread.[25] The dominating fast bush growth even occurred at $-0.5\ \mathrm{mA\,cm^{-2}}$ (last 3 s of supporting video SV5), but it was triggered after the deposition of a considerably larger amount of lithium than for the higher rates. For $-0.5\ \mathrm{mA\,cm^{-2}}$, approximately $4.1\ \mathrm{mAh\,cm^{-2}}$ were deposited after the pretreatment before the bush growth started, while it was only about $1.33\ \mathrm{mAh\,cm^{-2}}$ and $1.25\ \mathrm{mAh\,cm^{-2}}$ for $-2.5\ \mathrm{mA\,cm^{-2}}$ and $-5\ \mathrm{mA\,cm^{-2}}$, respectively. At a rate of $-10\ \mathrm{mA\,cm^{-2}}$, the fast bush growth initiated immediately after the start of the deposition.

Figure 3 gives an overview of characteristic morphologies of the lithium deposits obtained at different rates. After a deposition at $-0.05\ \mathrm{mA\,cm^{-2}}$ the electrode surface is covered by long needles but also by some lithium flakes with considerably larger dimensions than the diameters of the needles. Some of the needles have multiple kinks (some with high angles) and a few needles are connected to the electrode at both ends to form loops (Figure 3a and b). At rates of $-2.5\ \mathrm{mA\,cm^{-2}}$ and higher, deposition was localized, and large areas of the electrodes were not altered and still covered with a dense film of lithium spheres, which already grew during the pretreatment, as shown in Figure 1b and in the lower part of Figure 3g. Bush growth typically initiated at various locations but usually one or only a few bushes dominated the growth. This coincides with a drop in the cell overpotential (Figure 2). A high-resolution image of a small bush that grew at the beginning of the electrodeposition but stopped to grow when other bushes started to dominate the deposition can be seen in Figure 1b. Since the fast-growing bushes grew very large and hence were extremely fragile, large parts of them broke off the electrodes and could not be observed by SEM. Therefore, at the higher rates mainly smaller bushes that grew at the beginning of the deposition and the parts of the fast-grown bushes that were closer to the electrode surface and did not break off were imaged in the SEM. For the electrode on which lithium was deposited at a rate of $-2.5\ \mathrm{mA\,cm^{-2}}$, the large bush shown in Figure 2c partly broke off but significant parts remained on the electrode and could be imaged. Figure 3c shows the right edge of the parting of the cylindrical bush (Figure 2b). Here, the initially dense bush opened but the rapid growth did not occur at the edge of the resulting trench. Outside of the parting, columnar lithium needles are very densely packed. When looking at the trench it becomes apparent that the diameter of these columnar grown deposits reduces significantly towards
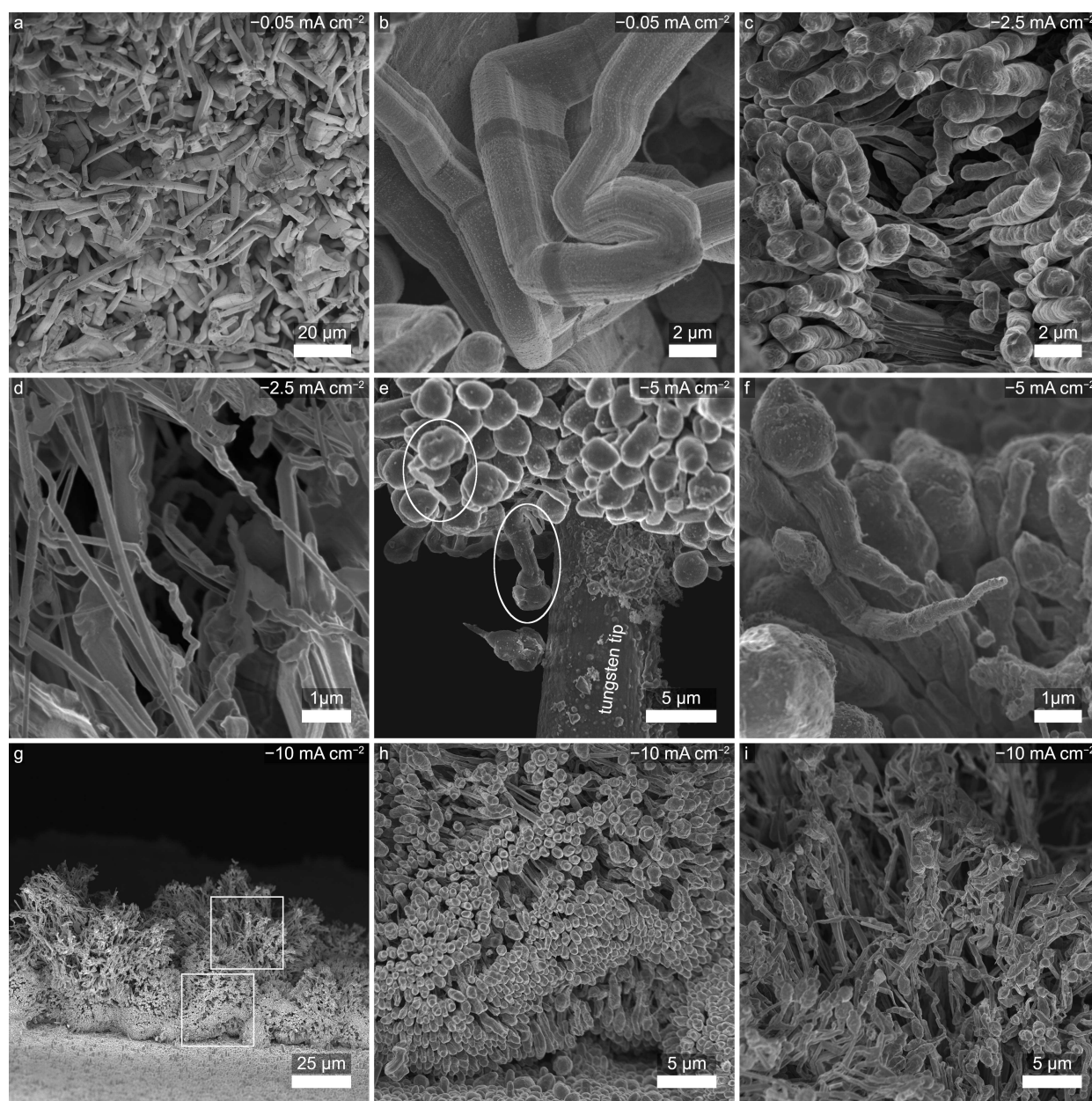
ChemElectroChem

Articles
doi.org/10.1002/celc.202100870

Chemistry Europe
European Chemical
Societies Publishing

Figure 3. SEM images after the electrodeposition of 5 mAh cm^{-2} at various rates. (a) Overview of the morphologies visible after the deposition at -0.05 mA cm^{-2} and (b) an exemplary needle with multiple high angle kinks. (c) Columnar grown deposits that form a dense structure, which parted open during the deposition at -2.5 mA cm^{-2} and (d) the structure in the inside of the fast grown bush at -2.5 mA cm^{-2}. (e) A dense Li bush grown at -5 mA cm^{-2} was mechanically opened with a tungsten tip on a micromanipulator. (f) Deposits inside of the bush after it was opened. (g) Overview of a fast grown bush at -10 mA cm^{-2} and a magnified from the dense lower part of the bush (h) und the upper part that is porous and unstructured (i). Focus stacking (see Experimental section) was used to increase the depth of field in image c (stack with four images) and d (stack with three images).

their base, resulting in shapes that share similarity to baseball bats. In order to better observe the inside of the fast grown bush (Figure 2c), we mechanically opened the remaining parts of the bush with a tungsten tip on a micromanipulator (Kleindiek Nanotechnik GmbH) inside the SEM. Figure 3d shows the inner part of the bush after opening it. The morphology of the deposits differs significantly to Figure 3c and appear much less uniform and less dense. Long fiber-like deposits with extreme aspect ratios and diameters partly below 100 nm grow next to deposits with diameters close to 1 μm. Furthermore,

some deposits have long facets, while others are kinked and almost crinkled. For the deposition at -5 mA cm^{-2} the bush that grew mainly in the first half of the deposition at the lower edge of the electrode (supporting video SV4) was examined. From the outside, the bush appeared very dense, and we again used the micromanipulator to examine the inside of the bush. Figure 3e shows a lithium deposit together with the tungsten tip that sticks inside. This reveals that deposits contain densely packed spheres at their outside and segments with smaller diameter behind them (highlighted by ellipses). Figure 3f was

ChemElectroChem

Articles
doi.org/10.1002/celc.202100870

**Chemistry
Europe**
European Chemical
Societies Publishing

recorded after parts of the bush had been scraped off. Generally, the morphology is similar to the one observed at $-2.5\ \text{mA}\,\text{cm}^{-2}$ (Figure 3c) with the difference that the diameter reduces abruptly behind the spherical tip instead of a more gradual reduction in diameter. Figuratively described: The shape resembles rather a tadpole than a baseball bat. For the deposition at a rate of $-10\ \text{mA}\,\text{cm}^{-2}$ the bush in Figure 3g-i has been identified to be representative for bush growth at high rate (Figure S3). The lower part of the bush close to the electrode surface (Figure 3h) is very dense and exhibits broader tips and has reducing diameters towards the inside of the bush. It is similar in morphology to Figure 3c and e. The upper part (Figure 3i) is less dense with very irregular shapes similar to the fast grown deposits in Figure 3d.

To summarize the different morphologies obtained with the variation of the deposition rate, Figure 4 compares the deposition of $1\ \text{mAh}\,\text{cm}^{-2}$, $2\ \text{mAh}\,\text{cm}^{-2}$, and $3\ \text{mAh}\,\text{cm}^{-2}$ at different rates. Each column of the image corresponds to one cell with a fixed deposition rate and each row contains images of these cells after the same amount of area specific charge. After the deposition of $1\ \text{mAh}\,\text{cm}^{-2}$ a roughened surface is visible at deposition rates of $-0.05\ \text{mA}\,\text{cm}^{-2}$ and $-0.5\ \text{mA}\,\text{cm}^{-2}$. For $-0.05\ \text{mA}\,\text{cm}^{-2}$ the first lithium needles just form, whereas at $-0.5\ \text{mA}\,\text{cm}^{-2}$ some short needles are clearly visible. In contrast

to the more evenly distributed deposits at lower rates, a preferred deposition at the upper and the lower edge of the electrode can be observed for $-2.5\ \text{mA}\,\text{cm}^{-2}$. At the highest rate of $-10\ \text{mA}\,\text{cm}^{-2}$, a fast three-dimensionally growing bush initiates at the beginning of the deposition and quickly dominates the deposition process. After the deposition of $1\ \text{mAh}\,\text{cm}^{-2}$ it already covers a significant part of the electrode. The out of focus area of this bush clearly shows growth towards the cell window, i.e. perpendicular to the direction towards the counter electrode. After the deposition of $2\ \text{mAh}\,\text{cm}^{-2}$, the electrodes are covered by needles for the lower rates of $-0.05\ \text{mA}\,\text{cm}^{-2}$ and $-0.5\ \text{mA}\,\text{cm}^{-2}$, but the needles are significantly longer for the lowest rate of $-0.05\ \text{mA}\,\text{cm}^{-2}$. In both cases small loops, i.e. kinked deposits that seem to be connected to the electrode at both ends, are visible (insets). At the rate of $-2.5\ \text{mA}\,\text{cm}^{-2}$, the bush at the upper edge parts open and a fast-growing bush started to grow (compare Figure 2). At $-10\ \text{mA}\,\text{cm}^{-2}$, the growth rate of the dominating bush seems to accelerate over time. After the deposition of $2\ \text{mAh}\,\text{cm}^{-2}$ the electrode depicted in the image is already fully covered with the bush that grew out of focus. After a deposition of $3\ \text{mAh}\,\text{cm}^{-2}$ the electrodes with the two lower deposition rates are still covered by needles, which are significantly longer at the rate of $-0.05\ \text{mA}\,\text{cm}^{-2}$. On both
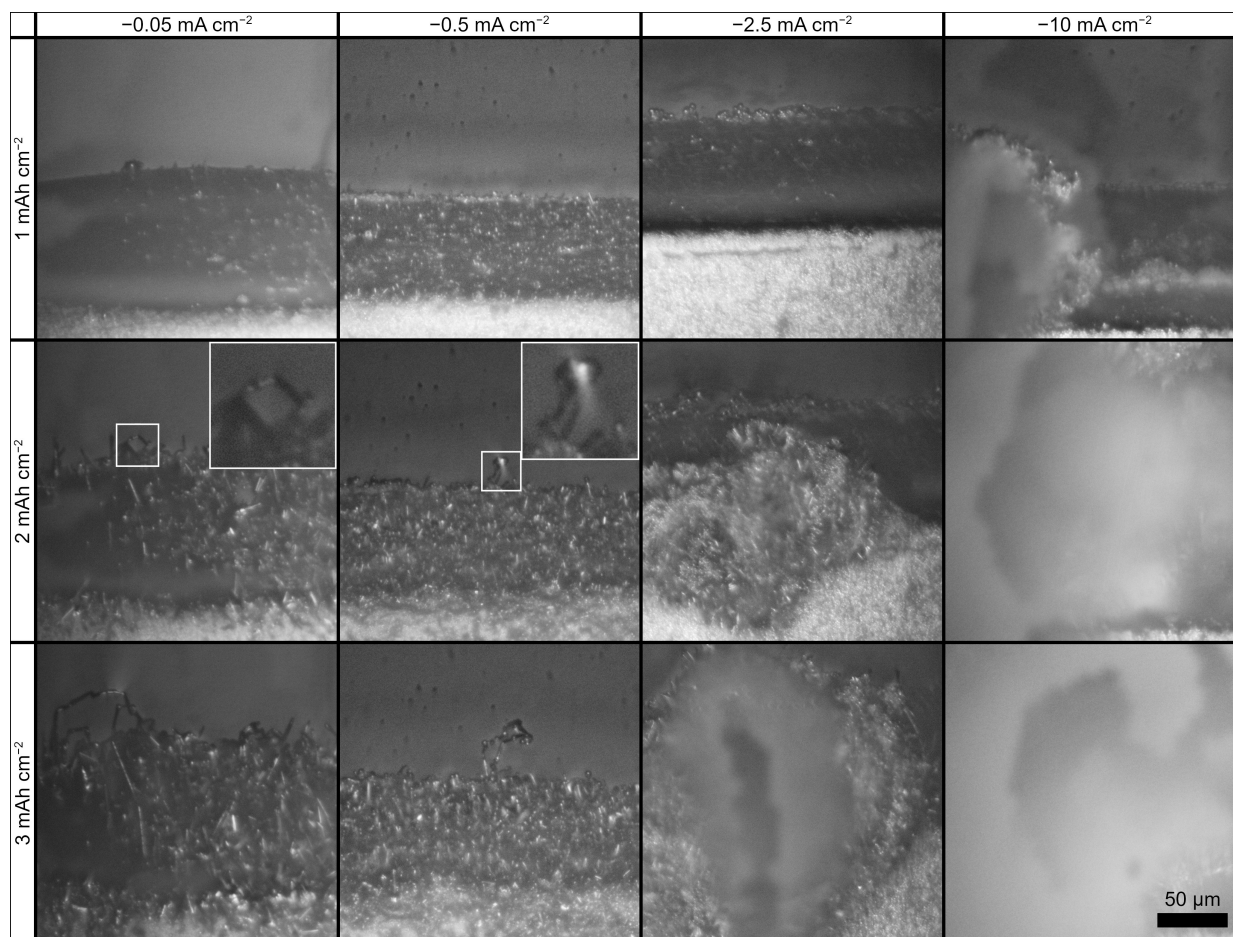

Figure 4. Comparison of the deposition of $1\ \text{mAh}\,\text{cm}^{-2}$, $2\ \text{mAh}\,\text{cm}^{-2}$, and $3\ \text{mAh}\,\text{m}^{-2}$ at $-0.05\ \text{mA}\,\text{cm}^{-2}$, $-0.5\ \text{mA}\,\text{cm}^{-2}$, $-2.5\ \text{mA}\,\text{cm}^{-2}$, and $-10\ \text{mA}\,\text{cm}^{-2}$.

electrodes, it is notable that loop-structures grow particularly fast. At the higher rates, the large bushes continue to dominate the growth and at -2.5 mA cm^{-2} the bush also starts to grow out of focus.

Higher current densities were applied in the modified test cell with a larger inter-electrode distance, and an objective with a lower magnification was used to ensure that the deposits did not grow out of the field of view. During the deposition at -50 mA cm^{-2} no significant differences in growth and the

galvanostatic voltage trace compared to the deposition at -10 mA cm^{-2} were observed. After the deposition of 16.7 mAh cm^{-2}, the current density was increased to -100 mA cm^{-2} and after slightly more than 4 min a sudden rise in the cell overpotential occurred, which is shown in Figure 5a. This behavior clearly indicates the depletion of ions close to the surface of the negative electrode.[13,14] Charge neutrality requires that both cations and anions change their concentration in the same way. After approximately 4.5 min the deposition changes
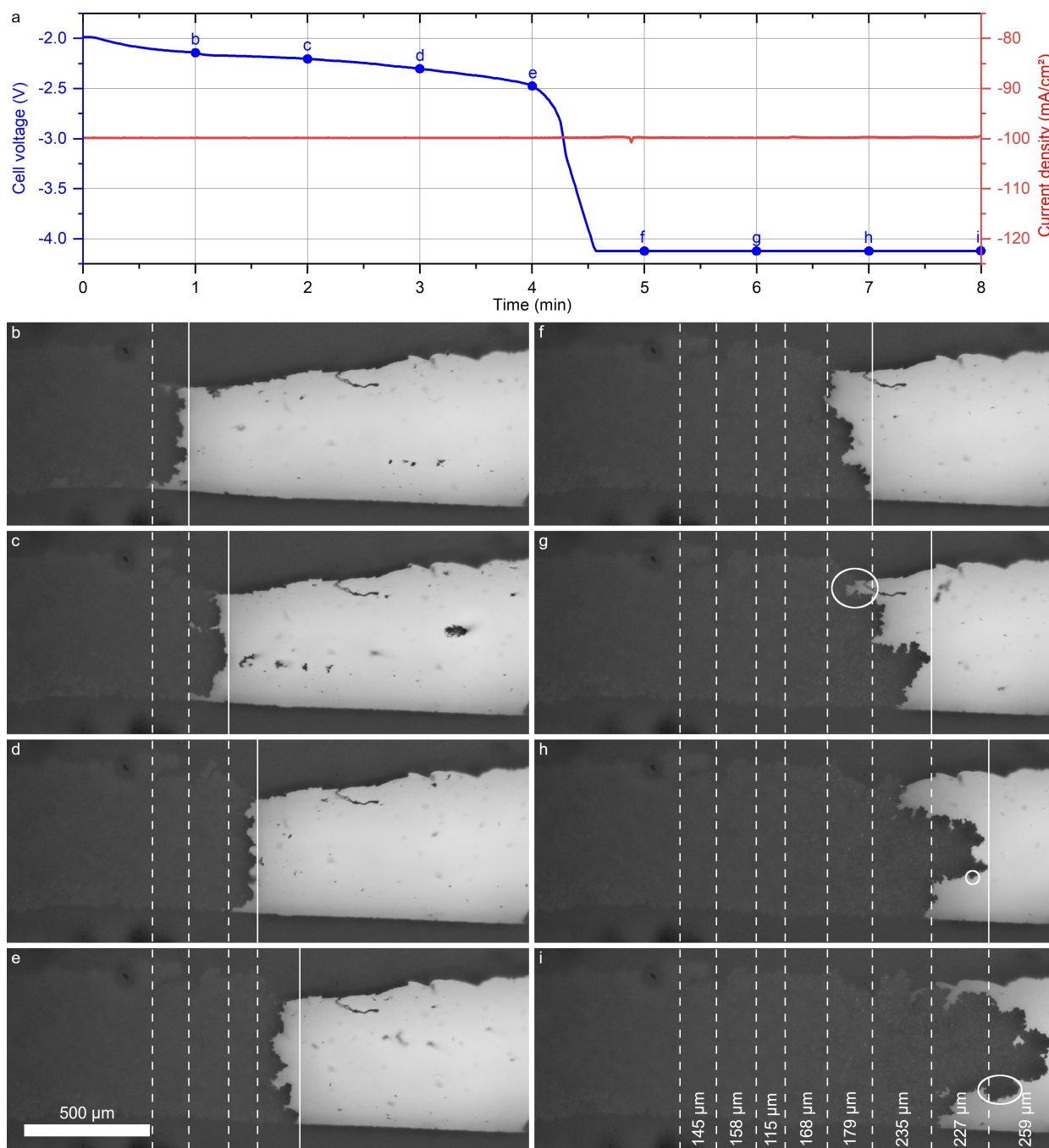

Figure 5. (a) Cell voltage at a deposition rate of -100 mA cm^{-2} with marks to indicate when the image stacks (b–i) were acquired. (b–i) Li bush that grows during deposition from the left side of each frame towards the right edge of the frames. The Dark areas at the top and bottom of each frame is the rubber sealing that borders the cell from all sides. The images were acquired after 1–8 minutes of deposition. The solid lines in all images mark the front of the Li bush and the dashed lines marks where the front of the bush was in the previous images.

ChemElectroChem

Articles
doi.org/10.1002/celc.202100870

Chemistry
Europe
European Chemical
Societies Publishing

to a potentiostatic lithium plating as the voltage range of the potentiostat of ± 4 V was reached. Nevertheless, the applied current was almost constant within the first 8 min of the deposition and hence the amount of plated lithium per minute was constant in the time span shown. Figure 5b-i show the cell during the deposition at -100 mA cm^{-2}. The time between the images is one minute. The solid lines in each image mark the front of the growing bush, while the dashed lines contain the deposition front of the previous images. The front of the bush moves between 115 μm and 259 μm per minute. Except at the front of the bush, the full width of the cell is visually covered by lithium. Furthermore, the height of the deposit exceeds the height of the electrode since the top of the deposit is mostly out of focus. Therefore, the lithium bushes at this high rate have to be very porous since only 1.67 mAh cm^{-2}, corresponding to a dense lithium film of 8.1 μm, are deposited per minute. The bush grows by 586 μm within the first four minutes of the deposition and by 900 μm within the following four minutes, clearly showing that the electrolyte depletion accelerates the growth. However, no distinctive change in the growth mechanism is apparent in our setup. Surprisingly, even after the depletion of the electrolyte, the deposition does not solely occur at the tip of the growing bush. The gap between the lithium and the rubber seal (surrounded by a white line in Figure 5g) is closed in Figure 5h and i despite being far from the tip of the deposition. Furthermore, the feature surrounded by the white lines in Figure 5h and i clearly indicates that growth does not only occur at the tip. The feature is pushed towards the counter electrode, demonstrating the growth that occurs behind this feature. The growth of the feature itself is also not directional towards the counter electrode as one might expect, it grows partly even in the opposite direction, towards the negative electrode. The backward growth can be best seen in video SV6. The video also shows particles that break off from the lithium counter electrode due to its fast dissolution. The motion of these floating particles may be used to infer on convection in the electrolyte.

The large bush broke apart when the cell was opened and washed in dimethyl carbonate (DMC). A transmission electron microscopy (TEM) grid was used to collect various parts from the disconnected deposits. Three SEM images with increasing magnification of an exemplary bush can be found in the supporting information (Figure S4a–c). Just as the other bushes, this bush exhibits a hierarchical structure. This can be seen by comparing Figure S4a and b which look similar despite the about ten times higher magnification. Even at this rate, the basic elements of the bush are needles and flakes (Figure S4a–c). The needles appear to be shorter than the ones found at lower rates and short needles and flakes are sometimes hard to distinguish. Figure S4d shows a different region of the deposit where the needle-like shapes are more pronounced. These needles are kinked and have facets. The facets are even more notable on the larger flakes. It appears that at short range, the deposits are quite densely packed. Voids exist in agglomerates of these densely packed units and there is an increasing size of voids when the agglomerates get larger. This results in a loosely

packed porous and hierarchical structure. In this respect, we do not see a conceptual difference to bushes grown at lower rates.

3. Discussion

Lithium was electrodeposited at different rates. Between the slowest and the most accelerated conditions, the deposition rate was varied by a factor of 2000 and consequently differences in the morphology of the deposits appeared. Surprisingly, also many similarities were found in the deposits and in the growth mode. At low rates, the deposits can be described by a homogeneous distribution of needles that grow from the base. With increasing current density, the deposition became less homogeneous, and bushes of interconnected needles grew at various sites. After a certain time or due to further increasing the rate, an abrupt transition from the growth of these dense bushes to fast growing individual porous bushes was commonly found. The highest rates caused a sudden increase in the cell overpotential. Even at these extreme conditions, no significant change in the growth mode was found. Based on our visual observations, we infer on the dominant mechanisms of growth and relate our findings to models available in the literature.

3.1. Variation of Rates and Resulting Morphologies

The deposition rate was varied between -0.05 mA cm^{-2} and -100 mA cm^{-2}. At the lowest rates, mainly individual needles grew evenly distributed over the whole electrode surface from the lithium spheres that were deposited during the pretreatment (supporting videos SV1 and SV5). These needles have facets, indicating crystalline growth with different growth rates along different crystal directions. At early stages, the needles clearly grow from the base, but with longer deposition times, an increasing number of kinked needles and loops appear that also grow between kinks. This indicates a growth mechanism based on the insertion into defects as suggested before.[23] The defects can be in the SEI and/or in the underlying lithium metal. SEI defects might be inhomogeneities in the chemical composition, cracks, or small regions that are very thin. In the lithium, the defects are associated with kinks, which typically contain grain boundaries, i.e. small regions that contain high amounts of dislocations and vacancies. A defect in the SEI and in the lithium crystal might be linked: e.g., the SEI on top of a grain boundary could differ from the one that forms on top of a perfect lithium crystal. This is plausible because the SEI varies depending on the orientation of the underlying lithium.[29] As already observed by Yamaki et al.,[21] crystalline defects (tips and kinks) can control later stages of growth. They and others[22,30] attribute the early growth of the whiskers to the release of mechanical stresses and the extrusion of metal. In our opinion, this mechanism is not required to nucleate needles as can be seen from experiments where needles directly grow on copper and from experiments where needles form during physical vapor deposition without SEI and electrochemistry.[27]

ChemElectroChem

Articles
doi.org/10.1002/celc.202100870

**Chemistry
Europe**
European Chemical
Societies Publishing

When comparing the deposition at low rates of $-0.05\ \text{mA cm}^{-2}$ and $-0.5\ \text{mA cm}^{-2}$, it is striking that the individual needles at $-0.05\ \text{mA cm}^{-2}$ grow considerably larger when equal charge is applied. It is plausible that during very slow deposition, defects in the SEI are less significant since the cracks in the SEI, which are inevitable when the lithium deposits grow, have enough time to heal by creating fresh SEI-layers. Therefore, at very low rates the crystalline growth of lithium appears to dominate the deposition. This supports the previously reported assumption that it is an intrinsic behavior of lithium to form needles at room temperature[27] and indicates that the growth of single crystalline lithium needles is favorable at the lowest deposition rates. As a consequence, concepts that solely use large electrode surface areas (porous nickel, porous copper, lithium particles, large surface area carbon) to reduce the effective current density, may not be effective in preventing needles. At higher rates, defects and inhomogeneities in the SEI might play an increasingly important role in the growth mechanism since their healing does not occur fast enough. This might also be the reason for the observed localized bush growth at rates of $-2.5\ \text{mA cm}^{-2}$ and higher. When lithium is deposited fast enough at a location where the SEI is thin and defective, fresh lithium surface is constantly generated, i.e. the SEI remains thin. This could result in a self-amplifying deposition mechanism and hence a deposition occurs on a decreasing number of bushes with increasing rate. Although the growth was observed to increasingly localize with increasing rate, the morphology of the individual deposits changes only slightly and still consists of the same building blocks: agglomerates of needles and some flakes. At higher rates, the deposits appear more disordered, ligament shapes become more rounded and less facetted, the diameters of the needles vary to a greater extent, and especially in dense bushes the diameter of individual needles changes significantly over their length. The ordered regular branching as is typical for example for solidification dendrites was not found in our experiments. The shape of the bushes suggests that branching rather is of statistical nature. We observed that lithium bushes, at all rates, grow non-directionally from the inside. This was already reported for low rates and compared to the raisin bread expansion model.[25] At lower rates, localized bush growth did not occur or only after the deposition of large amounts of lithium. However, the loops observed at low rates show a geometrically similar expansion since they grow between kinks and hence the kinks grow apart from each other. The growth of bushes from the inside and the growth between kinks are hard to explain by the well-known growth models based on effects of the substrate or ion depletion and electrical fields in the electrolyte. We therefore suggest defect-driven insertion as the dominating growth mechanism at all rates.

3.2. Abrupt Transition to Fast Bush Growth

For all cells with current densities between $-0.5\ \text{mA cm}^{-2}$ and $-5\ \text{mA cm}^{-2}$, a sudden transition to a localized fast bush growth was observed. For the lowest current density of $-0.05\ \text{mA cm}^{-2}$,

such a transition was not observed and for the higher current densities, these fast-growing bushes occurred already at the beginning of the deposition. In all cases, the transition of the growth mode coincided precisely with a drop in the overpotential, clearly demonstrating that ion depletion cannot be responsible for this transition. In one case, the bushes initiated at locations farthest from the counter electrode, excluding the possibility that a reduction of the inter-electrode distance causes the drop in overpotential. It is plausible that a fast-growing bush has not only more surface area, but also more crystalline defects at which lithium can be inserted into the deposits and hence reduces the effective current per defect, resulting in a lower resistance of the cell. Additionally, the SEI on these fresh and fast-growing deposits has to be thin and defective, resulting in a faster transport through the SEI at an increasing number of insertion locations. The almost ignition-like start of the fast bush growth is most likely triggered by sudden exposure of areas without a protective SEI layer. Since the cell geometry is not significantly altered due to the growth of this bush, the drop in overpotential (Figure 2d) is caused by larger electrode surface area with thinner SEI. This indicates that a relatively large fraction of the overpotential originated from the SEI and not only from the liquid electrolyte. The importance of the SEI for the growth of dendrites has been emphasized by Cohen et al.[19] and Aurbach et al.[31] According to our findings, the morphology of the deposits shows that they are crystalline. The size of the crystallites varies with rate, indicating that crystalline defects play a fundamental role in the growth. SEI also seems to contribute: Small-scale defects in the SEI but also in the underlying lithium are responsible for growth of needles with kinks, while larger cracks or delamination of SEI result in the onset of individual fast-growing bushes.

During the deposition at $-5\ \text{mA cm}^{-2}$, the fast-growing bushes initiate at the edge of the rubber seal that was placed on top of the copper block and SEM examination of the block revealed deposits underneath the rubber seal (supporting information Figure S5). We presume that before the fast growth was triggered, the seal had been slightly moved or lifted by the deposited lithium and hence the bare copper without a protective SEI was suddenly exposed, allowing the initiation of a fast and localized bush growth. Although this example is very specific to our cells, it clearly demonstrates the effect what happens when fresh surfaces are exposed. In real cells, this could be the delamination of protective films, the movement of a separator, or could happen when the so-called dead lithium breaks off. Furthermore, during the deposition at $-2.5\ \text{mA cm}^{-2}$, the fast growth was triggered on a thick layer of lithium that was deposited before and far away from all rubber seals. Here a dense lithium bush opens probably due to mechanical stress that developed during growth, and it is very likely that this results in considerable damage to the SEI. To the best of our knowledge, the correlation of the initiation of fast bush growth and a drop in the overpotential was not reported before, which is probably caused by two reasons. First, to detect this very localized phenomenon, the observation of large regions at high resolution is required. Second, at moderate rates this only happens after significant charge has been applied. In many

ChemElectroChem

Articles
doi.org/10.1002/celc.202100870

Chemistry Europe
European Chemical
Societies Publishing

deposition experiments, not enough lithium is deposited to detect this phenomenon. In cells with reasonable capacities (~ 3 mAh cm$^{-2[6]}$) this effect is expected to be detectable.

3.3. Ionic Depletion of the Electrolyte

The evolution and growth of dendrites is often attributed to the ionic transport within the electrolyte. Transport limitations are obviously relevant for highly diluted solutions as described by Chazalviel[9] and might be relevant for polymer electrolytes as discussed by Monroe and Newman.[15] The transport limitation is described by the limiting current density $J_{lim} = \frac{2z_c c_0 FD}{L(1-t_c)}$.[13–15] For our high rate cell with an inter-electrode distance of $L = 4.1$ mm, a cationic charge number $z_c = 1$, an initial salt concentration in the electrolyte of $c_0 = 1$ M, the Faraday's constant $F = 96485$ As mol^{-1}, a salt diffusion coefficient D in a range $2...4 \cdot 10^{-6}$ cm^2 s^{-1},[32–34] and a cationic transference number t_c in a range from 0.25 to 0.45,[32–34] the limiting current density J_{lim} is expected to be in the range $1.3...3.4$ mA cm^{-2}. No pronounced rise of the cell overpotential, as expected and reported for complete ion depletion,[13,14] was observed at a current density of -50 mA cm^{-2}, which is significantly higher than the calculated limiting current density. In the next step of the experiment, the current density was increased to -100 mA cm^{-2}. Due to the previous deposition at -50 mA cm^{-2}, the inter-electrode distance L reduced to approximately 2.6 mm at the beginning of the deposition with -100 mA cm^{-2} (relative to the original surface area) and hence the range for the expected limiting current density changed to $J_{lim} = 2.0...5.4$ mA cm^{-2}. The theoretical Sand's time

$$\tau_{Sand} = \pi D \left(\frac{z_c c_0 F}{2J(1-t_c)} \right)^2 {}^{[13,14,16]}$$ is between 2.6 s and 9.7 s for this experiment, but the observed increase in cell potential occurred after approximately 4 minutes. Sand's behavior did not occur at the calculated limiting current density. Instead, it occurred only for higher current densities and significantly later than calculated. This is expected as convection is not negligible in experimental cells with large volumes of liquid electrolyte. Convection is evident in our cells (supporting video SV6), although the cell is relatively narrow and has a volume that was estimated to be below 3.25 µl. Bai et al.[14] performed experiments with larger inter-electrode distance and significantly smaller electrode surfaces in cells that even reduce their diameter towards the middle of the cell. It seems plausible that with their extreme dimensions, convection is almost negligible and hence their experimentally measured Sand's time is closer to the calculated one.

We have observed – even after the cell overpotential rose abruptly – a deposition of lithium that is not very directional and does not solely occur at the tip of the deposits. This growth inside the lithium structure (instead of at locations closest to the counter electrode) does not coincide with any model previously reported in literature, where severe depletion inevitably induces tip growth. This indicates that the deposition of lithium is far more complex than described by these models, which are usually based on a one-dimensional ion depletion zone. Moreover, these observations imply that concepts that aim in preventing tip growth[35] may not be effective for preventing dendrites. Even at the extreme conditions with a cell potential of -4 V, where electrolyte depletion is certainly present, the observed deposition does not appear to be dominated by the transport limitations in the liquid electrolyte. A possible explanation for the observed behavior is a very complex geometry of the three-dimensional depletion zone in the electrolyte, which is presumably not homogeneous and not stationary due to the growing structure in combination with convection in the electrolyte. If the electrolyte is not fully depleted within a few small spots, lithium can be deposited from there. If these spots are small, no significant drop in the overpotential would be observed. The growth from the inside of the lithium bushes indicates that even at these extreme conditions the growth mechanism is still governed by the insertion into defects and hence a deposition is not possible at any location of a lithium bush. Since the SEI is inevitably thin on the surfaces of fast-growing bushes, the SEI may not define preferred insertion sites and crystalline defects seem to play an important role in the growth mechanism. One might also imagine that the growth of lithium can occur in regions of ionic depletion due to the surface diffusion of lithium atoms. In this case, the first step of lithium deposition, the electron transfer, happens at another place than the crystallization. This atom diffusion mechanism could explain growth sites in some limited distance away from the electrochemically active sites.

In summary, we observed no significant change in the growth mechanism despite the ionic depletion within the electrolyte.

3.4. Implications for Real Cells

The electrodeposition of lithium is important for future lithium metal secondary batteries where it is part of the operating principle but also very critical in the current lithium-ion technology, where lithium dendrites are considered to be a safety risk. In our experiments, it was hardly possible to reach ion depletion in commonly used liquid electrolytes for lithium-ion batteries for all current rates that are relevant for practical applications. Even when we forced ion depletion during our *operando* observations, it had only minor impact on the growth mode. Bai et al.[14] demonstrated depletion and fractal growth at considerably lower current densities. These differences in the observations are probably caused by convection, which might be negligible in the capillary cells of Bai *et al.* In commercial cells, separators probably suppress convection completely. However, the inter-electrode distance in commercial cells is two to three orders of magnitudes smaller than in the capillary cell of Bai *et al.*, resulting in significantly higher limiting current densities. To estimate the impact of ion depletion in commercial cells, the limiting current density was calculated for an exemplary high power 18650 lithium-ion cell. For the Sony VTC5A cell, used for this calculation, the limiting current density was more than 100 times higher than the maximum continuous charge current density for this cell (see supporting information

A6). Therefore, Sand's behavior seems to be irrelevant for practical cells with liquid electrolytes. This suggests that initiation and growth of the notorious dendrites in lithium-ion cells is not controlled by concentration gradients in the electrolyte. In contrast to the hardly relevant ion depletion, the fast-growing lithium bushes, which can already occur at lower deposition rates, are likely to play a very crucial role and might be the main safety concern of lithium-ion cells and an obstacle in the commercialization of lithium metal anodes in rechargeable batteries. The porous bushes exhibit large surface areas and hence result in a significant electrolyte consumption. Furthermore, they result in an extreme volume expansion, causing mechanical stresses within the cell. Separators damaged by large structures and not by single needles have recently been investigated.[36] A major problem is the formation of dead lithium during discharge[25] and a sufficient Coulomb efficiency seems hardly possible when lithium is deposited as bushes.

4. Conclusions

Operando light microscopy at the physical resolution limit of light was used to obtain a clear picture of growth modes during electrodeposition of lithium from a liquid electrolyte. The aim of this study was to identify the rate dependence of the growth. An almost flat deposition of lithium spheres was achieved for the deposition of 0.5 mAh cm^{-2} during the pretreatment and at lower rates for another 0.5…1 mAh cm^{-2}. However, after the deposition technologically relevant amounts of charge, a flat deposition could not be achieved at any rate in the carbonate-based electrolyte (EC (ethylene carbonate)/DMC). In the experiments, the rates were varied by a factor of 2000 and different deposits grew at different rates. The shapes of the deposits vary, but despite the large rate variations, they also show similarities. At all rates a large amount of facetted elements can be found in the deposits, indicating crystalline lithium growth. For very low rates, the deposits consist of needles that are quite evenly distributed across the electrode. For increased rates, the needles become shorter and contain more kinks. Lithium insertion happens at the base and at kinks. These sites are defects in the crystalline lithium structure but also in the SEI that probably alleviate lithium insertion. This leads to facetted crystalline lithium segments, which are building blocks of the growing structures. Further increasing the rate causes the formation of bushes that grow from their inside and still contain facetted and kinked elements. In this regime, growth can abruptly localize onto an individual bush that then dominates the whole deposition process. Our results suggest that the exposure of surfaces without SEI can trigger this transition. Here the defects in the SEI are probably considerably larger as the other type of SEI defect, which is found in the altered SEI on top of a kink in a facetted needle. Fresh metal can be exposed by the movement of cell components, delamination of the SEI, or the breakage of a deposit. Bushes, which are based on the crystalline building blocks, are the dominating lithium structures up to highest rate. Even when the voltage indicates ionic depletion within the electrolyte, bushes dominate electrodeposition, and their growth mode does not change. This suggests that for the safety of real cells the depletion of cations and the localization of growth onto an individual protrusion is not as relevant as accelerated bush growth.

Experimental Section

As working electrodes, copper blocks were cut from a 0.5 mm thick foil (99.9999% Puratronic foil from Alfa Aesar). These blocks were ground and polished (last polish with a grit size of 4000) to the desired shape as shown in Figure 6. The front side facing towards the lithium metal counter electrode is ground at an angle of approximately 10 ° to improve the observation of nucleation and the initial growth and has a surface area of about 0.3 to 0.4 mm². Since this was ground manually, the blocks vary to a certain degree in size and shape. Their surface can exhibit a slight curvature, which in combination with the illumination in the microscope can lead to variations in brightness in the images/videos. To remove trace oxides from the copper surface, the blocks were heated to approximately 250 °C in a glove box antechamber in a forming gas atmosphere (5% H$_2$ und 95% Ar) at 2 mbar. A piece of lithium (99.9% from Alfa Aesar) was used to form the counter electrode. All cells were filled with a commercially available electrolyte (1 M LiPF$_6$ (lithium hexafluorophosphate) in a 1:1 volume ratio mixture of EC and DMC) from Merck.

The *operando* microscopy cells were assembled inside an argon-filled glove box (H$_2$O and O$_2$ content typically < 0.1 ppm). A schematic of a cell is shown in Figure 6. For each cell a sapphire plate was used as substrate and two copper foils (10 μm, >99.95% from h+s Präzisionsfolien GmbH) were attached to the substrate as current collectors. Lithium was pressed onto one current collector as counter electrode. The shape of the electrodes and the electrolyte compartment was cut into a flat rubber sealing and the working electrode was clamped into the slit of the rubber to
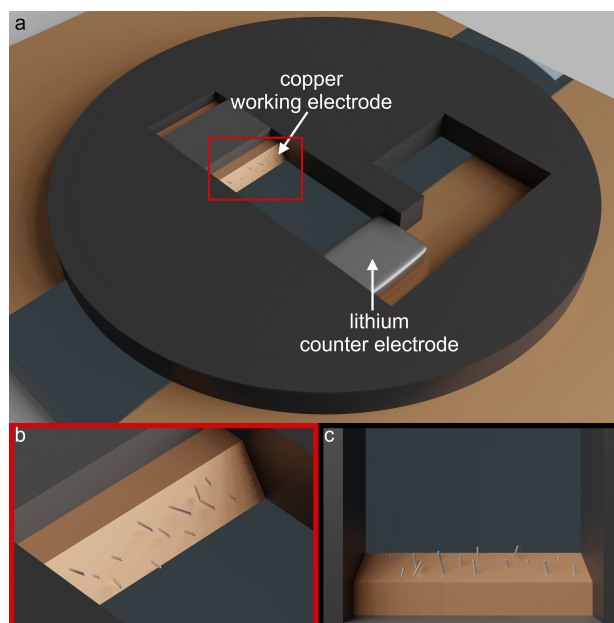

Figure 6. (a) Schematic of microscopy cell in 3D view. Magnification of the working electrode with needle-like lithium deposits (b) and the working electrode in top view as observed with the light microscope during *operando* measurements (c).

prevent deposition at the sides of the copper block. Another small piece of the rubber was placed on top of the copper block to prevent plating there and to press the block down onto the current collector. The rubber could not be placed directly at the edge of the copper block since it would block the view onto the deposition area when the cell is sealed and the rubber compressed. In addition to the tilted surface facing the counter electrode, deposition is only possible on a small stripe on the top side of the block. After filling the cell with electrolyte, the cells were sealed by clamping the sapphire substrate and a sapphire window between two metal plates. For additional investigations, selected cells were disassembled in a glove box and after washing in DMC, the copper blocks with the lithium deposits were transferred into a SEM, using a vacuum transfer system (Leica EM VCT 100).

The *operando* light microscopy was performed with a Nikon Eclipse LV-UDM in bright field mode. To increase the depth of field, image stacks with typically more than 100 images were acquired. An objective scanning system with a piezo drive (Physik Instrumente (PI) GmbH & Co. KG) was used the fast acquisition of image stacks. A stack with 100 images could be completed within a timespan as short as about 10 s, enabling the *operando* observation at high deposition rates. With this optimized setup, it is possible to observe sample volumes of up to 0.27 mm^3 at a high resolution close to the physical resolution limit of light (~500 nm). The images with an extended depth of field were then calculated from the z-stacks with an algorithm based on Laplacian pyramids,[37] using a GPU for faster computation of the large stacks and large number of stacks. This method has the additional benefit that the stacks contain three-dimensional information in addition to the two-dimensional projections acquired by conventional light microscopy.

A potentiostat (CompactStat.e, Ivium Technologies B.V.) was used for the galvanostatic deposition of lithium onto the copper working electrode. To create a dense lithium film on the copper electrodes, a 30 s seeding step for the nucleation at -5 mA cm^{-2} followed by the deposition of 0.5 mAh cm^{-2} at a rate of -0.5 mA cm^{-2} was performed on every cell after assembly. Typically, additional 5 mAh cm^{-2} of lithium were deposited at different rates between -0.05 mA cm^{-2} and -10 mA cm^{-2} in each cell directly after this pretreatment. For even higher rates, the lithium deposits grow quickly out of the field of view and might short circuit the cell after a short period of time. Therefore, the test cell was modified by increasing the inter-electrode distance and the *operando* observation of the growth was observed with an objective with a lower magnification to apply deposition rates of -50 mA cm^{-2} and -100 mA cm^{-2}.

Acknowledgements

Conflict of Interest

The authors declare no conflict of interest.

[1] J.-G. Zhang, W. Xu, W. A. Henderson, *Lithium Metal Anodes and Rechargeable Lithium Metal Batteries*, Springer International Publishing, Cham, Switzerland, **2017**.
[2] D. Lin, Y. Liu, Y. Cui, *Nat. Nanotechnol.* **2017**, *12*, 194–206.
[3] X. B. Cheng, R. Zhang, C. Z. Zhao, Q. Zhang, *Chem. Rev.* **2017**, *117*, 10403–10473.
[4] Z. Xie, Z. Wu, X. An, X. Yue, J. Wang, A. Abudula, G. Guan, *Energy Storage Mater.* **2020**, *32*, 386–401.
[5] J. H. Um, S. H. Yu, *Adv. Energy Mater.* **2020**, *11*, 2003004.
[6] P. Zou, Y. Sui, H. Zhan, C. Wang, H. L. Xin, H. Cheng, F. Kang, C. Yang, *Chem. Rev.* **2021**, *121*, 5986–6056.
[7] T. Foroozan, S. Sharifi-Asl, R. Shahbazian-Yassar, *J. Power Sources* **2020**, *461*, 228135.
[8] B. Liu, J. G. Zhang, W. Xu, *Joule* **2018**, *2*, 833–845.
[9] J. N. Chazalviel, *Phys. Rev. A* **1990**, *42*, 7355–7367.
[10] C. Brissot, M. Rosso, J. N. Chazalviel, P. Baudry, S. Lascaud, *Electrochim. Acta* **1998**, *43*, 1569–1574.
[11] M. Rosso, T. Gobron, C. Brissot, J. N. Chazalviel, S. Lascaud, *J. Power Sources* **2001**, *97–98*, 804–806.
[12] H. J. S. Sand, *London, Edinburgh, Dublin Philos. Mag. J. Sci.* **1901**, *6*, 45–79.
[13] C. Brissot, M. Rosso, J. N. Chazalviel, S. Lascaud, *J. Power Sources* **1999**, *81–82*, 925–929.
[14] P. Bai, J. Li, F. R. Brushett, M. Z. Bazant, *Energy Environ. Sci.* **2016**, *9*, 3221–3229.
[15] C. Monroe, J. Newman, *J. Electrochem. Soc.* **2003**, *150*, A1377–A1384.
[16] A. R. Despic, K. I. Popov, in *Mod. Asp. Electrochem.* (Eds.: B. E. Conway, J. O. Bockris), Springer US, Boston, MA, **1972**, pp. 199–313.
[17] J. L. Barton, J. O. Bockris, *Proc. R. Soc. A Math. Phys. Eng. Sci.* **1962**, *268*, 485–505.
[18] R. Akolkar, *J. Power Sources* **2013**, *232*, 23–28.
[19] Y. S. Cohen, Y. Cohen, D. Aurbach, *J. Phys. Chem. B* **2000**, *104*, 12282–12291.
[20] K. N. Wood, E. Kazyak, A. F. Chadwick, K. H. Chen, J. G. Zhang, K. Thornton, N. P. Dasgupta, *ACS Cent. Sci.* **2016**, *2*, 790–801.
[21] J. I. Yamaki, S. I. Tobishima, K. Hayashi, K. Saito, Y. Nemoto, M. Arakawa, *J. Power Sources* **1998**, *74*, 219–227.
[22] A. Kushima, K. P. So, C. Su, P. Bai, N. Kuriyama, T. Maebashi, Y. Fujiwara, M. Z. Bazant, J. Li, *Nano Energy* **2017**, *32*, 271–279.
[23] J. Steiger, D. Kramer, R. Mönig, *J. Power Sources* **2014**, *261*, 112–119.
[24] H. Park, O. Tamwattana, J. Kim, S. Buakeaw, R. Hongtong, B. Kim, P. Khomein, G. Liu, N. Meethong, K. Kang, *Adv. Energy Mater.* **2020**, *11*, 2003039.
[25] J. Steiger, D. Kramer, R. Mönig, *Electrochim. Acta* **2014**, *136*, 529–536.
[26] O. Crowther, A. C. West, *J. Electrochem. Soc.* **2008**, *155*, A806–A811.
[27] J. Steiger, G. Richter, M. Wenk, D. Kramer, R. Mönig, *Electrochem. Commun.* **2015**, *50*, 11–14.
[28] K. W. Desmond, E. R. Weeks, *Phys. Rev. E - Stat. Nonlinear, Soft Matter Phys.* **2009**, *80*, 051305.
[29] Y. Zhang, V. Viswanathan, *Langmuir* **2020**, *36*, 11450–11466.
[30] X. Wang, W. Zeng, L. Hong, W. Xu, H. Yang, F. Wang, H. Duan, M. Tang, H. Jiang, *Nat. Energy* **2018**, *3*, 227–235.
[31] D. Aurbach, E. Zinigrad, Y. Cohen, H. Teller, *Solid State Ionics* **2002**, *148*, 405–416.
[32] C. Capiglia, Y. Saito, H. Kageyama, P. Mustarelli, T. Iwamoto, T. Tabuchi, H. Tukamoto, *J. Power Sources* **1999**, *81–82*, 859–862.
[33] L. O. Valøen, J. N. Reimers, *J. Electrochem. Soc.* **2005**, *152*, A882–A891.
[34] A. Nyman, M. Behm, G. Lindbergh, *Electrochim. Acta* **2008**, *53*, 6356–6365.
[35] F. Ding, W. Xu, G. L. Graff, J. Zhang, M. L. Sushko, X. Chen, Y. Shao, M. H. Engelhard, Z. Nie, J. Xiao, X. Liu, P. V. Sushko, J. Liu, J. G. Zhang, *J. Am. Chem. Soc.* **2013**, *135*, 4450–4456.
[36] K. L. Jungjohann, R. N. Gannon, S. Goriparti, S. J. Randolph, L. C. Merrill, D. C. Johnson, K. R. Zavadil, S. J. Harris, K. L. Harrison, *ACS Energy Lett.* **2021**, *6*, 2138–2144.
[37] W. Wang, F. Chang, *J. Comput.* **2011**, *6*, 2559–2566.